University of Hertfordshire UH

The Role of H-optimisation on the Computed Intermolecular Interactions and Charge Transfer Integrals in Diketopyrrolopyrroles

Jesus Calvo-Castro,[a] *Alan R. Kennedy,*[b] *and Callum J. McHugh*[c]

[a] School of Life and Medical Sciences, University of Hertfordshire, Hatfield, AL10 9AB, U.K.

[b] Department of Pure & Applied Chemistry, University of Strathclyde, Glasgow, G1 1XL, U.K.

[c] School of Computing, Engineering and Physical Sciences, University of the West of Scotland, Paisley, PA1 2BE, U.K.

*Corresponding author: j.calvo-castro@herts.ac.uk.

ABSTRACT: Small organic conjugated systems displaying one dimensional stacking motifs in the solid state that facilitate charge propagation are highly desirable. Non-covalent interactions, although weak, can synergistically provide those supramolecular architectures with large binding energies and associated thermal integrity. Amongst the plethora of intermolecular interactions contributing towards the overall lattice energy and stability of the charge propagation

supramolecular architectures, H-bonding interactions are well known to play a pivotal role. Despite their critical contribution, the positions of hydrogen atoms in X-ray crystallographic data are parameterised, which can lead to significant changes in the computed intermolecular interactions. Herein, we report for the first time, an analysis of the role that the optimisation of the H atoms in X-ray structures has on the computed intermolecular interactions energies in diketopyrrolopyrroles. A large dataset comprising 94 dimer pairs from 19 different DPP-based systems, including three pigment analogues, was employed. In total, more than 1400 H-X chemical bonds were considered and optimised using the M06-2X density functional at the 6-311G(d) level. Intermolecular interactions were computed for the H-optimised geometries and compared to those from non-optimised counterparts. We report that in 35 out of the 94 dimer pairs investigated (37%), that computed intermolecular interactions were at least 2.5 kJ mol^{-1} larger on progression to the H-optimised geometries. In turn, lower computed values were yielded upon H-optimisation were computed for 8 out of the 94 dimer pairs (8%), with one case exhibiting a difference greater than 2.5 kJ mol^{-1}. In line with the negligible changes to electron density and wavefunction overlap, the computed changes on the transfer integrals for hole and electron were always lower than 1 kJ mol^{-1}. The observed changes to computed intermolecular interactions can play a critical role in determining the thermal integrity of the supramolecular structures and charge propagation channels, and thus in the absence of neutron diffraction data, H atoms should be optimised prior to computation. We envisaged that the results herein will be of interest to the extensive scientific community devoted to the understanding of intermolecular interactions in organic conjugated systems and the realisation of superior charge transfer mediating materials, and given the plethora of intermolecular interactions investigated, are not solely limited to those exploiting diketopyrrolopyrrole-based architectures.

INTRODUCTION

The contribution of hydrogen atoms to intermolecular interactions (ΔE_{CP}), which are not solely restricted to H bonds, is ubiquitous in chemical and biological systems. These interactions are known to play a key role in defining the strength of the overall intermolecular interactions and associated conformational changes in a number of processes from protein binding interactions to charge transfer mechanisms in optoelectronic materials.[1–8] Accordingly, accurate determination of their location around heavy atoms in molecular systems is widely acknowledged to play a key role in the fundamental understanding of such interactions that can ultimately lead to the development and engineering of superior alternatives. Accurate determination of the lengths of chemical bonds bearing H atoms and their exact location does not represent a trivial task, particularly using routine X-ray diffraction instrumentation, and is somewhat limited to less available neutron diffraction facilities.[9–13] Consequently, considerable efforts have been devoted to the development of novel approaches that can be routinely implemented to X-ray diffraction data to yield comparable results to those obtained by neutron diffraction.[9,11,13–18] Among these different approaches, free refinement of the hydrogen atom coordinates by an independent atom model is known to result in X-H distances which are shorter than those obtained by neutron diffraction analyses. Subsequently, the use of aspherical atomic scattering factors instead of the more commonly used independent atom model in the refinement in the Hirshfeld Atom Refinment (HAR) model has demonstrated to represent a superior alternative.[17,18] Another approach is to place the hydrogen atoms according to previous refinement criteria, leading however to inaccurate positions, particularly in molecular systems where the environment (i.e. presence of strong inter- and/or intramolecular H bonds) denotes a significant contribution. In an aim to improve X-ray diffraction data in relation to the position of the hydrogen atoms, some approaches employ neutron diffraction data to accurately

locate their position, either by constraining the positions in the refinement to those obtained by neutron diffraction or by elongating the X-H bond lengths to values obtained by neutron diffraction. However, if the hydrogen atoms are involved in significant stabilising interactions, the yielded geometry is still inaccurate. More recently, methodologies based on theoretical calculations have been exploited, with observed results that are in good agreement to those obtained by neutron diffraction.[9,11]
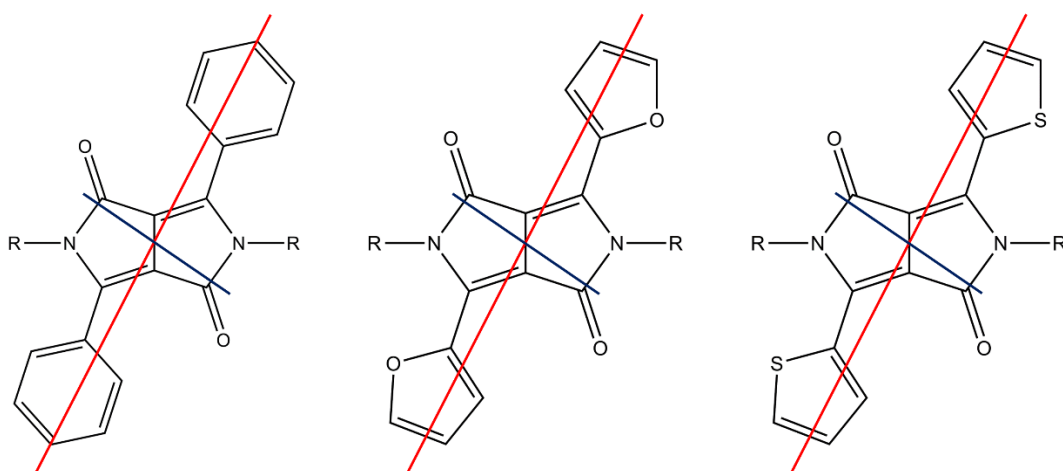
Figure 1. Diketopyrrolopyrrole structures bearing phenyl (left), furan (centre) and thiophene (right) core rings. Red and dark blue solid lines illustrate the long and short molecular axes respectively.

Whilst the development of novel approaches for the accurate location of hydrogen atoms from X-ray diffraction data still denotes a field of active research, to the best of our knowledge there remains a lack of understating on the effect that these optimisations may bear on the theoretical calculation of intermolecular interactions and associated properties, such as charge transfer integrals, in small conjugated organic materials. Along these lines, we are particularly interested in the realisation of superior diketopyrrolopyrrole (DPP) based platforms (Figure 1) that can find

applicability as charge transfer mediating materials in optoelectronic devices, whereby the charge transfer properties are strongly influenced by the formation of one-dimensional π-π supramolecular stacking motifs which serve as desirable charge propagation channels.[19–24] Experimentally observed supramolecular architectures as well as their integrity; critical in the design and realisation of optimum performers due to the reported sensitivity of transfer integrals to small intermonomer displacements, is determined by intermolecular interactions that in most cases are X---H in nature.[5–7,21] In this regard, it is of particular note that even in cases where the monomers within the one-dimensional supramolecular motifs are not significantly held together by intermolecular interactions involving H atoms, due to relative orientation of the monomers with respect to one another, the overall lattice stabilisation and thus the integrity of the charge propagation channels is often controlled by intermolecular contacts that involve H atoms.

DPP based systems are often associated with close H-bonding intermolecular interactions between electronegative oxygen atoms in the core carbonyl groups and electropositive H atoms within the core rings and/or N-substituents. These type of interatomic contacts have also been observed to be largely responsible for the intermolecular interactions in other widely used organic materials such as perylenes and rubrene based materials.[6,7] Consequently, the location of the H atoms in small organic conjugated materials, can result in changes to the computed intermolecular interactions that can ultimately modify our understanding of their supramolecular arrangements, thermal integrity of desirable charge propagation channels and overall device performance.

Inspired by these findings and underpinned by our previous work on engineering novel DPP based materials by performing systematic and rational substitutions, we report an in-depth analysis on the role that the computational optimisation of H atom positions from X-ray diffraction data bears on the computed ΔE_{CP} and associated charge transfer energies in DPPs. Examination of the

Cambridge Structural Database (CSD) confirmed to us the absence of any neutron diffraction data on DPP architectures. Our study encompasses a comprehensive dataset comprising 94 different nearest neighbour dimer pairs from 19 distinct DPPs,[19–23,25–27] resulting in more than 1400 X-H bonds that are explored. In order to account for the different 'environments' of these interactions, optimisation of the H atom positions was carried out using dimeric systems and not the monomeric units. Additionally, transfer integrals for both hole and electron transfer were also computed for the optimised geometries and compared to those obtained for the non-optimised ones. In short, our work reveals that if neutron diffraction instrumentation is not available, the position of H atoms in X-ray geometries should be optimised prior to the computation of intermolecular interactions and that the use of M06-2X density functional[28] at 6-311G(d) level in dimeric and not monomeric systems denotes a preferred approach. Out of the 94 dimer pairs investigated, in 35 of them (37%) we observed differences in ΔE_{CP} on progression from X-ray to H-optimised geometries greater than 2.5 kJ mol^{-1}, with one case exhibiting an increase of more than 10 kJ mol^{-1}. In turn, 8 out of the 94 dimer pairs investigated were characterised by a decrease in the intermolecular interaction upon H-optimisation. However, in all cases bar one, that energy difference was observed to be lower than 2.5 kJ mol^{-1}. Lastly, following the optimisation of the H atoms, changes lower than 1 kJ mol^{-1} in the computed charge transfer integrals were observed in all cases, in line with the negligible changes to electron density and wavefunction overlap. Importantly, and in relation to the large number of different types of intermolecular interactions evaluated in this work, we anticipate our findings to be of interest and transferable to those engaged in the judicious design and subsequent development of novel architectures bearing core motifs other than the DPP one.

The rest of the paper is laid out as follows: firstly, we detail the computational methodology employed in the optimisation of the H-atoms and the subsequent theoretical determination of

intermolecular interaction and charge transfer integrals in all investigated dimer pairs. We dedicate the first part of the Results and Discussion section to the examination of the effects of H-optimisation on reported DPP pigments. This is subsequently followed by the investigation of a series of N-substituted DPPs: i) symmetrical and asymmetrical architectures bearing halogen atoms on the para position of the core phenyl rings, ii) systems characterised by isosteric fluorine substitutions and iii) N-benzyl and N-alkyl systems exhibiting heteroaromatic substitutions on the core rings. The last part of this section is devoted to the observed effects on the computed charge transfer integrals upon H-optimisation. Finally, we summarise our conclusions.

EXPERIMENTAL SECTION

Optimisation of H atom positions. The optimisation of the H atoms was carried out by freezing the position of all the heavy atoms and leaving the H atoms to freely optimise their position. In all cases, X-ray geometries were employed as the starting point of the H-optimisation calculations and all calculations were performed on crystal derived dimer supramolecular architectures and not the monomeric units (*vide supra*). The H-optimisation calculations were carried out by means of M06-2X density functional[28] at 6-311G(d) level as implemented in Spartan 10 software.

Intermolecular interaction energies, ΔE_{CP}. Upon optimisation of the position of the H atoms in the dimeric architectures, the intermolecular interaction energies were calculated and compared to those previously reported by us for their non H-optimised counterparts. For consistency, we used Truhlar's M06-2X[28] density functional at the 6-311G(d) level as implemented in Spartan 10 software.[29] All computed intermolecular interactions were corrected for Basis Set Superposition Error (BSSE) following the method described by Boys and Bernardi,[30] which can be expressed as:

$$\Delta E_{CP} = E_{AB}^{AB} - E_{A}^{AB} - E_{B}^{AB}$$

where E_{AB}^{AB} denotes the energy of the dimer pair in the dimer basis and E_A^{AB} and E_B^{AB} represent the energy of the monomers (A and B) in the dimer pair basis.

Charge transfer integrals, $t_{h/e}$. The transfer integrals for both, hole (t_h) and electron (t_e) were computed within the framework of the energy splitting in dimer method,[31] which can be written as:

$$\Delta E_{AB} = \sqrt{(E_A - E_B)^2 + 4t_{AB}^2}$$

where E_A, E_B represent the site energies of the monomers A and B and t_{AB} the charge transfer integral of the AB dimer pair. Herein, due to computational limitations, we only report the charge transfer integrals for centrosymmetric dimer pairs where the site energies of the monomers in the dimer pair are identical. As such, t_h (t_e) can be equated to half the splitting between the HOMO (LUMO) and HOMO-1 (LUMO+1) supramolecular orbitals of the dimer pair. These calculations were performed employing the M06-2X density functional[28] at the 6-311G(d) level, as implemented in Spartan 10 software.[29]

RESULTS AND DISCUSSION

Computed intermolecular interactions, ΔE_{CP} in DPP-based pigments. The different solubility of DPPs in organic solvents when comparing pigment with dye analogues is widely known to be associated to strong intermolecular H bonding interactions between electronegative carbonyl oxygen atoms and electropositive amide hydrogens, which are disrupted upon N-substitution.[32–34] Consequently, it was of interest to evaluate the effects of H-optimisation on the computed intermolecular interactions in the three DPP pigments investigated, namely **HDPP**,[26] **ClDPP**[25] and **PDPP**,[27] with names in the form of **XDD** where **X** denotes the substitution on the para position of the phenyl core rings (i.e. P = phenyl).
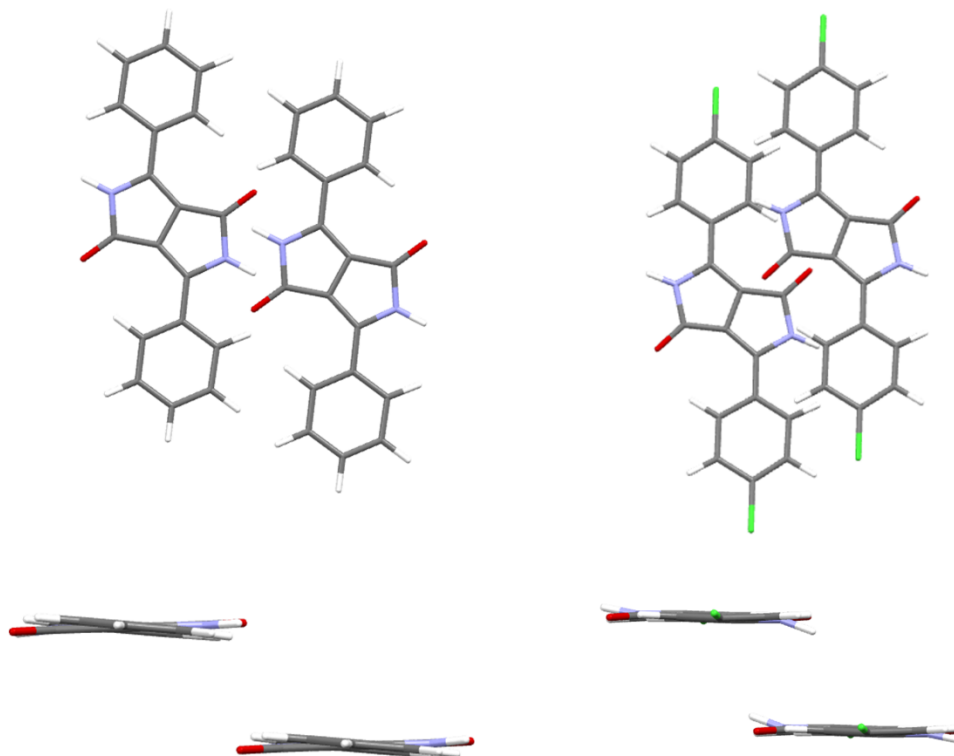
Figure 2. Capped stick illustration of the dimer pair II and IV of ***HDPP*** (left) and ***ClDPP*** (right) along the x (top) and z (bottom) molecular axes.

Two out the five nearest neighbour dimer pairs in **HDPP** were observed to exhibit variations in ΔE_{CP} greater than 2.5 kJ mol^{-1} on progression from X-ray to H-optimised geometries. In both cases, H-optimisation led to greater ΔE_{CP} in both dimer pairs (6.31 and 3.93 kJ mol^{-1} for dimer pair I and II respectively, SI2), primarily ascribed to the shortening of the O---H interactions (1.816/1.801 and 3.038/2.846 Å for the X-ray/H-optimised of dimer pair I and II respectively). In the case of dimer pair II of **HDPP**, due to the intermonomer displacement along the short molecular axis, the interatomic contact involves the ortho phenyl H atom and not the amide one. Halogen substitution on the para position of the core phenyl rings leads a significantly different packing motif in ***ClDPP***.[25,26] We observed that only one out of the five nearest dimer pairs is characterised by a change in ΔE_{CP} exceeding 2.5 kJ mol^{-1} upon H optimisation (dimer pair IV, 4.59 kJ mol^{-1}). As

opposed to dimer pair II of **HDPP**, the greater stabilisation cannot be associated to closer H-bonding interactions but to a number of enhanced dipole-dipole interactions in the slipped co-facial dimer pair arrangement, facilitated by the smaller displacement along the short molecular axis[5] (5.47 and 4.08 Å for dimer pair II of **HDPP** and dimer pair IV of **ClDPP** respectively). Interestingly, in the case of the biphenyl analogue of **HDPP**, **PDPP**, the largest increase in the computed intermolecular interaction of all investigated systems on optimisation of the H atoms was computed. Whilst dimer pairs I and II for **PDPP** exhibit greater stabilisations in line with those observed for **HDPP** and **ClDPP**, the computed ΔE_{CP} for dimer pair II was 19.00 kJ mol^{-1} greater upon H-optimisation (SI2). However, after careful evaluation we ascribed this large energy difference to issues in the quality of the crystal structure, particularly in relation to the CHN angles and the positions of the H atoms and cannot attribute it solely to a result of the H optimisation carried out.

Computed ΔE_{CP} in end-capped halogen substituted DPPs. On progression to soluble DPPs, obtained by carrying out substitutions on the lactam nitrogen atoms, the above described C=O---H-N intermolecular interactions are disrupted (Figure 2). Nonetheless, an important component of the total lattice binding energy is attributed to intermolecular interactions that involve electronegative carbonyl oxygen atoms (*vide infra*). Simultaneously, N-substitution results in changes to the packing motifs and the emergence of one-dimensional π-π stacking supramolecular architectures affording desirable charge propagation channels.[5]

Table 1. Intermonomer displacements and computed intermolecular interactions, ΔE_{CP} for X-ray and H-optimised π-π dimer pairs of **HBDPP**, **ClBDPPα**, **ClBDPPβ**, **BrBDPP**, **IBDPP**, **mBrBDPP** and **mIBDPP**.

DPP	Δx / Å	Δy / Å	Δz / Å	ΔE_{CP} / kJ mol^{-1}		
				X-ray	**H-optimised**	**% difference**
HBDPP	4.52	0.05	3.44	-70.12	-77.44	10.44
ClBDPPβ	5.13	0.28	3.38	-69.60	-77.62	11.52
ClBDPPα	9.39	1.22	3.22	-42.51	-46.13	8.52
BrBDPP	8.44	0.05	3.37	-39.46	-44.05	11.63
IBDPP	9.40	0.31	3.32	-35.52	-37.96	6.87
mBrDPP	3.57	0.23	3.42	-79.16	-86.08	8.74
mIBDPP	3.55	0.05	3.66	-79.36	-87.25	9.94

Within the series of halogenated N-benzyl substituted DPPs,[21,22] all of which conform to one dimensional π-π stacking motifs where the degree of intermonomer slip is controlled by the halogen substitution, it was interesting to observe that in all cases, computed ΔE_{CP} were larger by more than 2.5 kJ mol^{-1} (2.44 kJ mol^{-1} for the π-π dimer pair of **IBDPP**) on progression from X-ray to H-optimised geometries of the π-π dimer pairs. These systems were given names in the form of **XYDPP**, where **X** and **Y** denote the substitutions on the para positions of the core rings and lactam nitrogen atoms respectively.
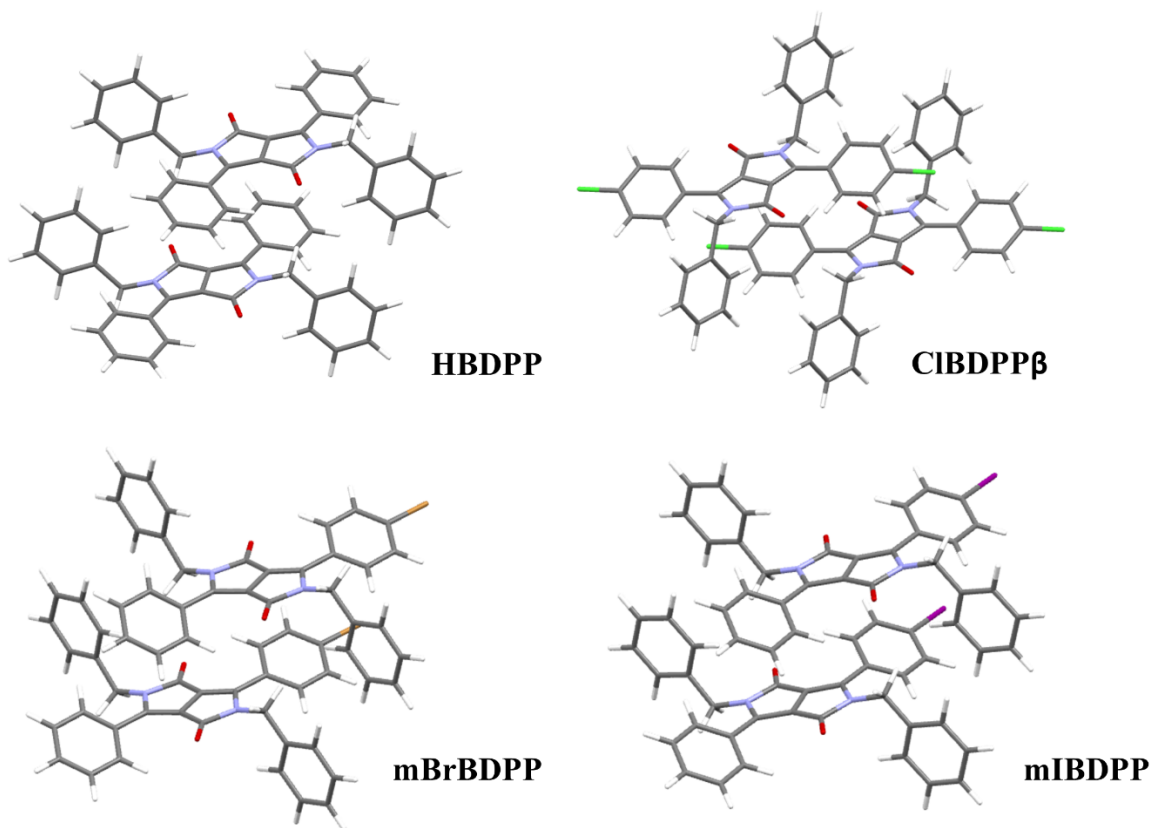
Figure 3. Capped stick illustration of the π-π dimer pairs of ***HBDPP***, ***ClBDPPβ***, ***mBrBDPP*** and ***mIBDPP***.

Via analysis of the data summarised in Table 1, it was apparent that greater increases in the intermolecular interaction upon H-optimisation were computed for those dimer pairs characterised by smaller shifts along their long molecular axes. In the case of ***HBDPP*** and ***ClBDPPβ***, this can be primarily attributed to intermolecular H-bonding interactions between electronegative carbonyl oxygen atoms and methylene protons as well as a meta hydrogen within the core phenyl rings, as illustrated in Figure 3, which become closer upon H-optimisation (O---H (methylene) of 2.850/2.734 and O---H (meta) 3.069/2.976 Å for X-ray/H-optimised geometries of ***HBDPP*** and ***ClBDPPβ*** respectively) The closer long molecular axes alignment in the case of the π-π dimer

pairs of **mBrBDPP** and **mIBDPP** results in more distanced interatomic contacts between the carbonyl oxygens and methylene protons than those observed in the π-π dimer pair of **HBDPP** (3.280/3.187 and 3.213/3.108 Å for **mBrBDPP** and **mIBDPP** respectively). However, closer O---H (meta) were observed in the case of the two mono-halogenated systems when compared to **HBDPP** and **ClBDPPβ** (3.053, 2.976, 2.806 and 2.807 Å for the H-optimised π-π dimer pairs of **HBDPP**, **ClBDPPβ**, **mBrBDPP** and **mIBDPP** respectively) which affords similar increases in computed ΔE_{CP} upon H-optimisation (see Table 1).

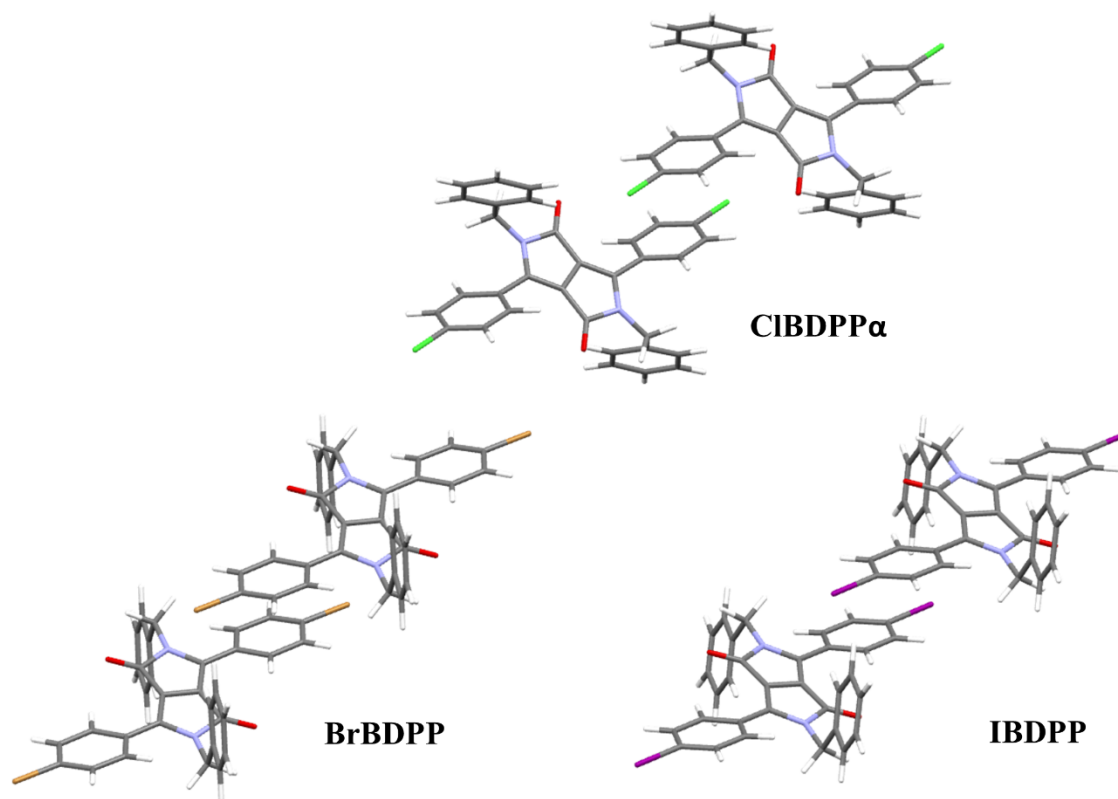**Figure 4**. Capped stick illustration of the π-π dimer pairs of **ClBDPPα**, **BrBDPP** and **IBDPP**.

In turn, a lower increment in ΔE_{CP} on progression to H-optimised geometries was observed for those dimer pairs characterised by larger intermonomer displacement along their long molecular axes, namely **ClBDPPα**, **BrBDPP** and **IBDPP**, where stabilising H-bonding interactions are either

absent (i.e. **BrBDPP** and **IBDPP**) or weaker (**ClBDPPα**) than those described for π-π dimer pairs more closely aligned along the long molecular axis. The increase in ΔE_{CP} for the H-optimised geometry in the case of the **BrBDPP** and **IBDPP** systems can be attributed to enhanced dipole-dipole interactions between the overlapping core phenyls for the elongated C-H bonds on H-optimisation as illustrated in Figure 4. Interestingly, close O---H (meta) and Cl---H (ortho) interatomic contacts are afforded in **ClBDPPα**, facilitated by the larger intermonomer slip along the short molecular axis ($\Delta y = 1.22$ Å) despite the similar Δx to **IBDPP** ($\Delta x = 9.39$ and 9.40 Å for the π-π dimer pairs of **ClBDPPα** and **IBDPP** respectively) where analogous interactions were absent. The smaller increase in the ΔE_{CP} observed upon H-optimisation for **ClBDPPα** than for its β polymorph (ΔE_{CP} = -42.51/-46.13 and -69.60/-77.62 kJ mol^{-1} for X-ray/H-optimised geometries of α and β polymorphs of **ClBDPP** respectively) despite the closer interatomic contacts in their optimised geometries (i.e. O---H (meta) of 2.861 and 2.976 Å for the α and β polymorphs respectively), can be accounted for on the basis of the additional stabilising intermolecular interactions that are absent in the alpha polymorph (i.e. H-bonding interactions involving methylene H atoms and additional dipole-dipole interactions between the conjugated cores which are stronger upon elongation of the C-H bonds in the H-optimised geometries). The latter illustrates that optimisation of H atoms based upon X-ray geometries is important, even in cases where strong close O---H intermolecular interactions are not responsible for the stabilisation of supramolecular architectures.

Computed ΔE_{CP} in fluorine-containing DPPs. Materials with superior performance are highly sought after and their identification has motivated material scientists worldwide to explore novel substitutions. The use of isosteric fluorine-hydrogen substitutions in small conjugated systems has attracted increased interest and has been reported for a number of small conjugated systems with

views of exploiting them in optoelectronic devices as charge transfer mediating materials.[19,20,35–41] Along these lines, we have previously reported DPPs whereby the systematic isosteric fluorine-substitutions resulted in significant changes to the packing motifs and therefore to the nature of the stabilising intermolecular interactions.[19,20] Irrespective of the supramolecular architecture of these fluorine-containing systems, it was observed that fluorine atoms engaged in a number of weak interatomic interactions, such as C-F---H, C-F---π_F and C-F---π, and not strong H-bonding interactions despite the large electronegativity of fluorine.[42–47]

Dimer pair III   **Dimer pair IV**
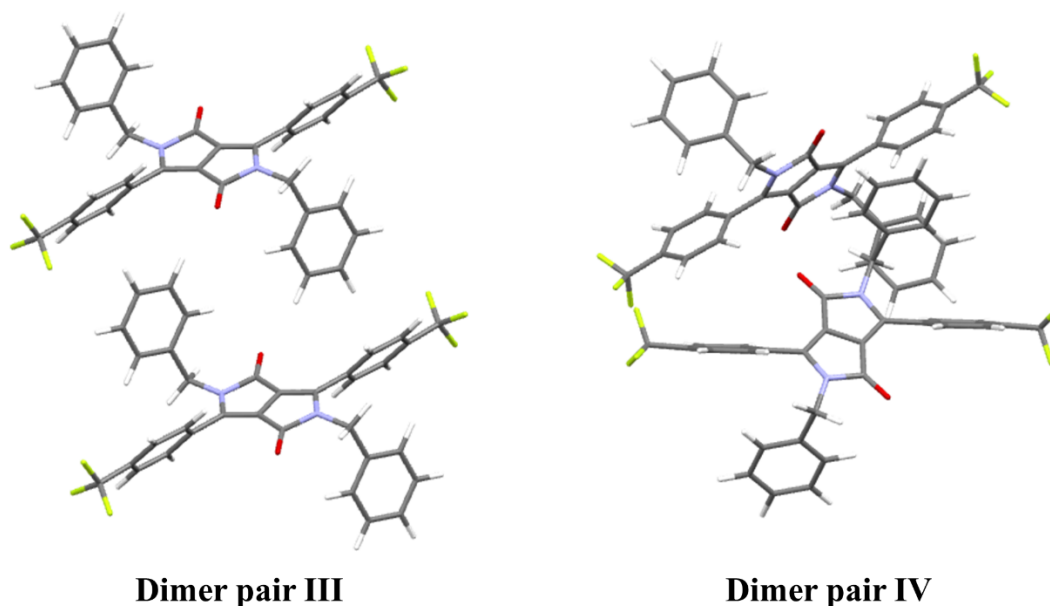
Figure 5. Capped stick illustration of the dimer pairs III (left) and IV (right) of ***THHBDPP***.

Herein, we explored the effect of H-optimisation on the computed ΔE_{CP} on these fluorine-substituted systems, namely ***THHBDPP***, ***THFBDPP***, ***HFFBDPP*** and ***HFHBDPP***.[19,20] These were adorned names in the form of **XYZDPP**, where **X** and **Y** represent the substitutions on the para (T = -CF$_3$) and meta positions of the core phenyl rings, respectively. In turn, **Z** denotes isosteric substitution of the phenylic hydrogen atoms for fluorine atoms within the benzyl groups.

15

It is of note that, unlike the findings described for the halogenated series (*vide supra*), only two of the π-π dimer pairs of the F-containing systems investigated exhibited an increase in the computed intermolecular interaction upon optimisation of the H atoms. In the case of the π-π dimer pair of **THHBDPP**, this can be attributed to the very large intermonomer slip along the long molecular axis ($\Delta x = 14.80$ Å), which precludes any close interatomic contact involving H atoms (Figure 5). Similarly, the long Δx slip in **HFFBDPP** ($\Delta x = 9.13$ Å), leads to highly separated intermonomeric contacts that result in negligible additional stability upon H-optimisation. Nonetheless, two out of the four nearest neighbour dimer pairs of **THHBDPP** do exhibit increments in their computed ΔE_{CP} upon H-optimisation that exceed 2.5 kJ mol^{-1}. In this regard, it is of interest that whilst in the case of dimer pair IV this can be solely ascribed to O---H (ortho) contacts at 2.638 and 2.520 Å in X-ray and H-optimised geometries, the additional stabilisation observed in dimer pair III results is attributed to the synergistic effect of O---H (meta) and F---H (para) that are shorter upon elongation of the respective C-H bonds (2.811/2.682 and 2.979/2.898 Å for O---H and F---H distances in X-ray/H-optimised dimer geometries respectively).
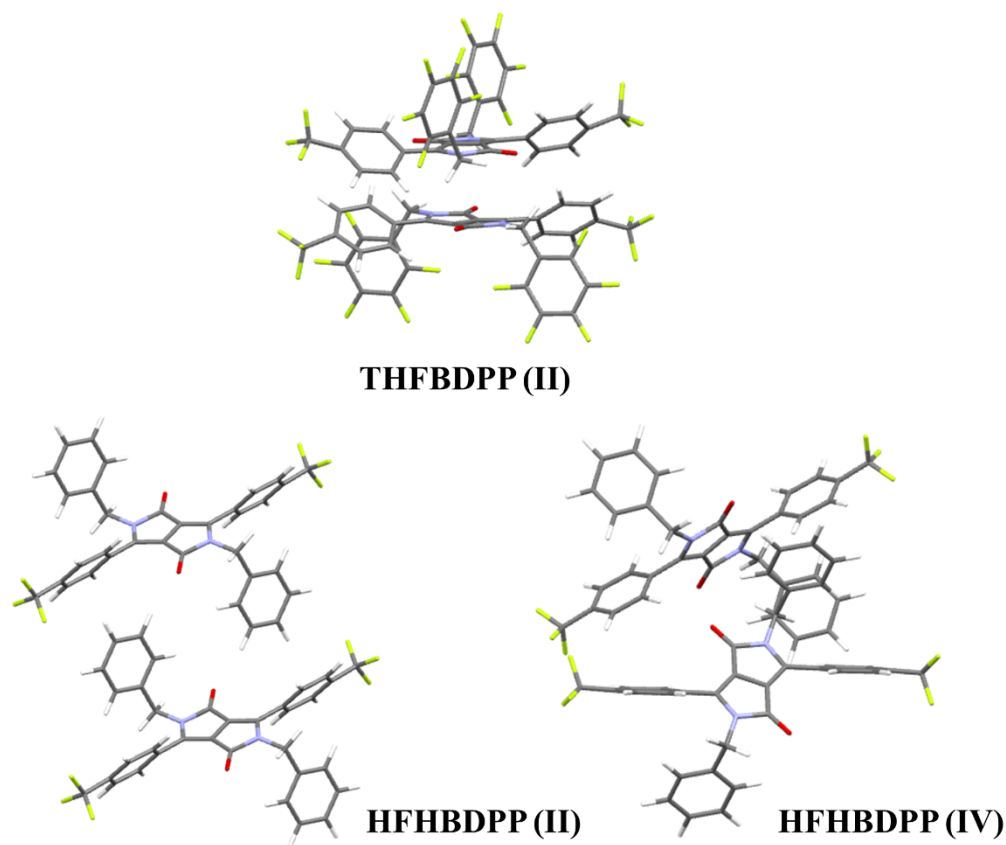
Figure 6. Capped stick illustration of the π-π dimer pairs of **THFBDPP** (II) and **HFHBDPP** (II and IV).

In turn, larger ΔE_{CP} were computed upon H-optimisation for the π-π dimer pairs of **THFBDPP** and **HFHBDPP**. The latter exhibits a 'classic' slipped-cofacial π- π dimer (IV) and a dimer pair (II), characterised by the overlap of the core rings in a 'head-to-tail' relative orientation as illustrated in Figure 6. Both of the dimer pairs in **HFHBDPP** are characterised by larger ΔE_{CP} (3.38 and 5.89 kJ mol^{-1} for dimer pair II and IV respectively, SI2) on progression to their optimised dimer geometries. Larger stabilisation energies can be attributed to close contacts in both dimer pairs as a result of their unique intermonomer slips as illustrated in Figure 6 ($\Delta x/\Delta y/\Delta z$ = 10.08/3.13/2.99 and 3.72/0.35/4.05 Å for dimer pair II and IV of **HFHBDPP** respectively). The

greater ΔE_{CP} in dimer pair II is associated to close H-bonding intermolecular interactions between electronegative oxygen atoms and electropositive phenyl H atoms in the para positions of the core rings, which are shortened from 2.552 to 2.411 Å upon H-optimisation. In turn, the smaller Δx in dimer pair IV facilitates alternative short contacts, particularly F---H (methyl and benzyl) in nature, separated by 2.716 and 2.626 Å on progression to H-optimised geometries. The larger increase in the computed intermolecular interaction energy upon optimisation in the case of dimer pair IV is further attributed to a number of dipole-dipole interactions throughout the conjugated backbones, which are strengthened due to elongation of the C-H bond lengths (i.e. 0.990/0.950-0.951 and 1.093/1.082-1.087 Å for aliphatic/aromatic C-H bond lengths in the X-ray and H-optimised dimer geometries).
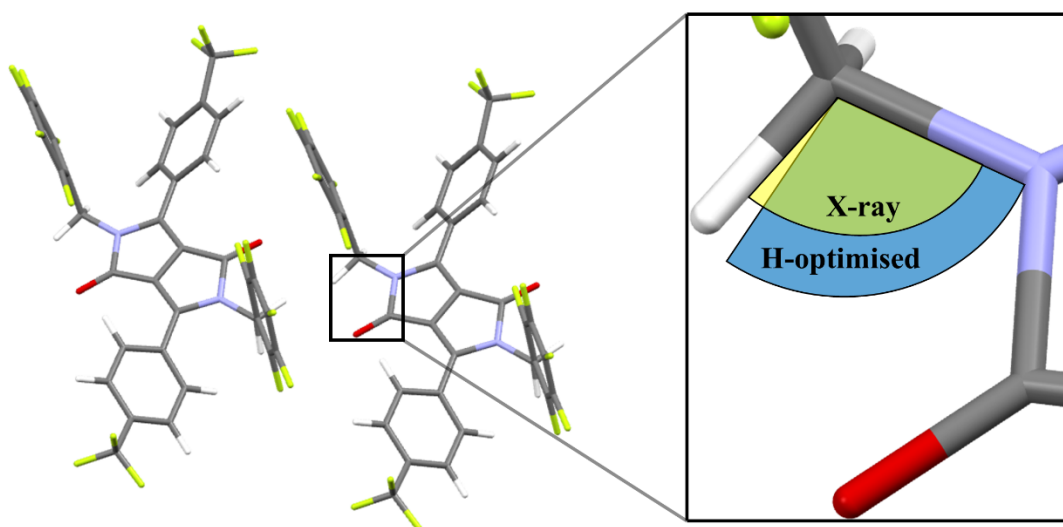

Figure 7. Capped sticks illustration of dimer pair III of **THFBDPP**.

In relation to the other structural analogue of the fluorinated series, **THFBDPP**, we report a decrease in the computed intermolecular interaction energy on progression to the H-optimised

dimer geometry (ΔE_{CP} = -38.55 and -33.37 kJ mol^{-1} respectively) for its dimer pair III (Figure 7). Upon examination of the optimised and non-optimised geometries, we observed a longer interatomic distance between the carbonyl oxygen atoms and methylene protons (2.801 and 2.842 Å in the X-ray and H-optimised dimer geometries of dimer pair III) despite the computed elongation of the C-H bond (0.990 and 1.085 Å respectively). In turn, the longer O---H interatomic distance observed upon H-optimisation can be attributed to a decrease in the H-C(methyl)-N angle from 108.43 to 103.92°. On the other hand, dimer pair II of ***THFBDPP*** exhibits a greater computed intermolecular interaction on progression to the H-optimised geometry, associated to the shortening of two weak H-bonding intermolecular interactions between carbonyl oxygens and methylene protons (2.612 and 2.530 Å on going to H-optimised geometry) and ortho-phenyl H atoms (2.914 and 2.795 Å in the X-ray and H-optimised geometries respectively), which are illustrated in Figure 6.

Computed ΔE_{CP} in heteroatom substituted DPPs. In tandem with systematic isosteric substitution of fluorine for hydrogen atoms on common core motifs in DPPs, heteroatom substitutions on the core rings as well as N-substituent effects have been explored in an effort to rationalise material properties with device performance.[21,23,48–50] We recently reported[23] that contrary to popular belief,[51] DPP systems bearing N-benzyl and phenyl core rings represent optimum theoretical alternatives for hole transport processes compared to furan and thiophene counterparts, despite the greater dihedral angle between these core rings and the DPP core.[23] Remarkably, large electron transfer integrals were computed for DPP systems bearing furan/thiophene core rings and long alkyl chains on the lactam nitrogen atoms, which further warrant the experimental determination of their mobilities in single crystal OFETs.

Table 2. Intermonomer displacements and computed intermolecular interactions for X-ray and H-optimised π-π dimer pairs of *HBDPP*, *FBDPP*, *TBDPP*, *HADPP*, *FADPP* and *TADPP*.

DPP	Δx / Å	Δy / Å	Δz / Å	ΔE_{CP} / kJ mol^{-1}		
				X-ray	**H-optimised**	**% difference**
HBDPP	4.52	0.05	3.44	-70.12	-77.44	10.44
FBDPP	4.11	1.78	3.38	-78.53	-83.71	6.60
TBDPP	2.96	3.26	3.45	-74.47	-79.78	7.13
HADPP	3.57	2.32	3.54	-59.94	-69.19	15.43
FADPP	3.57	0.15	3.31	-72.03	-74.32	3.18
TADPP	4.04	0.05	3.53	-65.45	-69.80	6.65

In relation to the computed ΔE_{CP} upon H-optimisation of their X-ray dimer geometries, we observe that in all cases the key π-π dimer pairs exhibit greater computed ΔE_{CP} upon H-optimisation (Table 2 for details). In N-benzylated systems, namely *HBDPP*, *TBDPP* and *FBDPP*, where T and F denote the use of thiophene and furan core rings instead of phenyl, an increase in the computed intermolecular interaction energies is primarily attributed to short O---H contacts (methylene in the case of *HBDPP* and *FBDPP* and ortho-phenyl in the case of *TBDPP*) that are shorter in H-optimised dimer geometries (2.850/2.734, 2.860/2.748 and 2.373 and 2.258 Å for H-optimised/X-ray dimer geometries of *HBDPP*, *FBDPP* and *TBDPP* respectively). The larger computed intermolecular interaction for the phenyl analogue can be accounted for on the basis of additional

dipole-dipole interactions between the core phenyl ring and the DPP core which are weaker in the π-π dimer pairs of **FBDPP** and **TBDPP** due to larger intermonomer displacements along their short molecular axes (see Table 2 for details and Figure 8). On progression to their N-alkyl substituted counterparts, the nature of stabilisation in the π-π dimer pairs is not necessarily attributed to stronger H-bonding interactions.
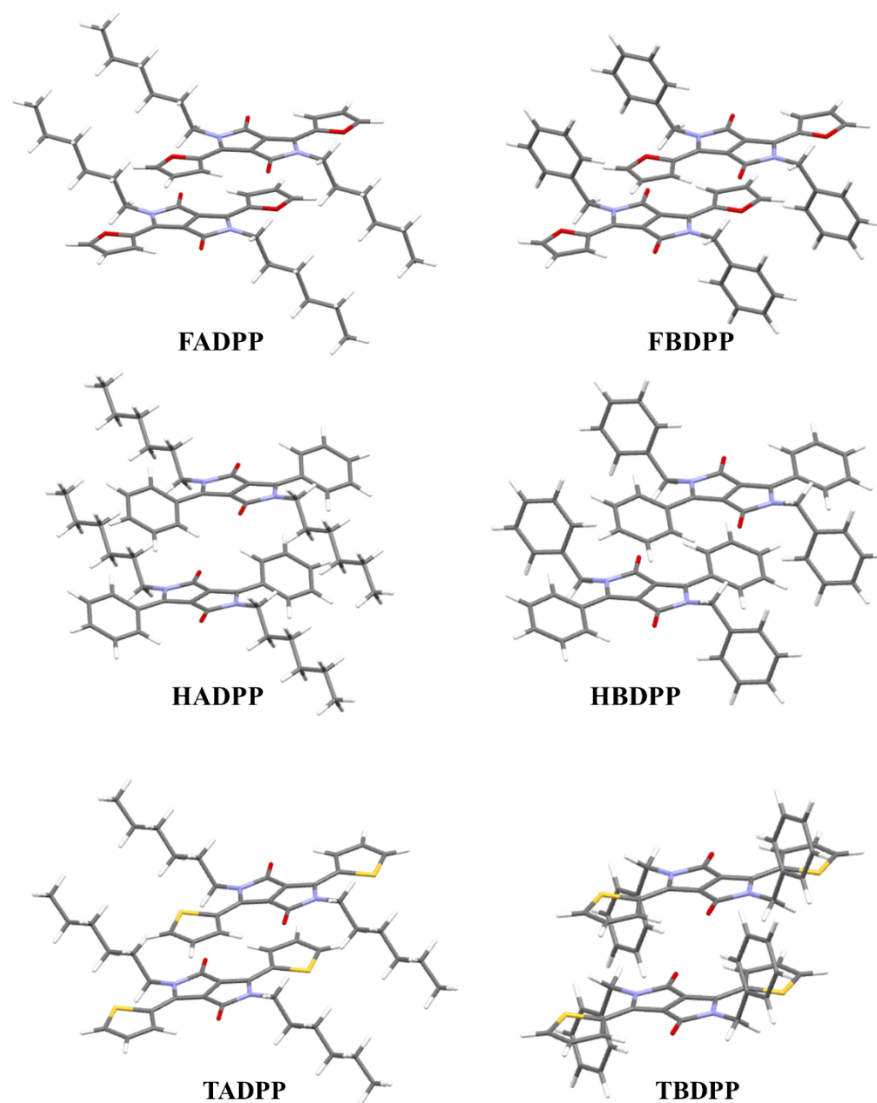

Figure 8. Illustration of the π-π dimer pairs of **HBDPP**, **HADPP**, **TBDPP**, **TADPP**, **FBDPP** and **FADPP**.

Whilst the π-π dimer pairs of **FADPP** and **TADPP** exhibit greater ΔE_{CP} upon H-optimisation which can be ascribed to O---H contacts that become shorter (2.819/2.720 and 2.895/2.742 Å for X-ray/H-optimised geometries of **FADPP** and **TADPP** respectively), the large increase (9.25 kJ mol^{-1}) in the computed ΔE_{CP} of **HADPP** (**PADPP** in the original publication[23]) was observed to be solely related to dipole-dipole interactions between C-H bonds (Figure 8) that are strengthened upon elongation of the C-H bond lengths (i.e. 0.930-0.931/1.084-1.085 and 0.960-0.971/1.092-1.099 Å for aromatic and aliphatic C-H bond lengths of X-ray/H-optimised geometries respectively). Accordingly, optimisation of hydrogen atoms in X-ray geometries prior to the theoretical calculation and evaluation of the intermolecular interactions is warranted even in those cases where the stabilisation of the dimer pairs does not involve stronger H-bonding interactions.

Computed charge transfer integrals, $t_{h/e}$. Lastly, we explored the effect of H-optimisation on the computed charge transfer integrals for the π-π dimer pairs. Hole and electron transfer integrals were computed for all centrosymmetric dimer pair systems contained in this study (56 out of the 94 dimer pairs investigated). We observed that, in all cases, the computed differences in the charge transfer integrals on progression from X-ray to H-optimised geometries was less than 1 kJ mol^{-1}, consistent with the negligible changes to the electron density and wavefunction overlap on elongation of the C-H bond lengths (SI2). However, in light of the reported large sensitivity of charge transfer integrals to small intermonomer displacements in small organic conjugated materials,[5,6,31] it is anticipated that optimisation of the hydrogen atoms prior to the calculation of ΔE_{CP} is critical in order to more accurately assess the thermal integrity of these systems and their charge propagation pathways.

CONCLUSIONS

In conclusion, we have reported for the first time an evaluation on the role that optimisation of the H atoms in X-ray structures of DPP based organic semiconductors has on their computed intermolecular interaction energies and charge transfer integrals. To do so, 94 nearest neighbouring dimer pairs from 19 different DPP-based architectures were evaluated, constituting a total of more than 1400 X-H interactions. The location of the H atoms was optimised by means of the M06-2X density functional at the 6-311G(d) level, and the results reveal than in 35 of these investigated dimer pairs, the computed intermolecular interaction energies on progression to H-optimised geometries were larger than these of their non-optimised counterparts by more than 2.5 kJ mol^{-1}. In most cases, these changes were ascribed to closer H-bonding interactions upon elongation of the H-X chemical bonds upon optimisation of the H atoms. We furthermore observed that in all cases but one, π-π dimer pairs that conform to desirable one-dimensional stacking motifs exhibited an increase in their computed intermolecular interactions in the H-optimised geometries; rationalised on the basis of the different intermonomer slips along both their long and short molecular axes. It was also observed that in π-π dimer pairs of systems bearing N-alkyl substituents (i.e. ***HADPP***), large increments in ΔE_{CP} on progression to optimised geometries were computed and attributed to strengthened dipole-dipole interactions between these side chains. Upon fluorination in the dimer pairs of ***THFBDPP***, a decrease in ΔE_{CP} was observed for the H-optimised dimer geometry, which was accounted for on the basis of the observed longer O---H distance despite elongation of the C-H bond, due to a structural rearrangement. Lastly, in line with the negligible changes to wavefunction overlap as a result of H-optimisation, changes in the computed charge transfer integrals lower than 1 kJ mol^{-1} were observed in all cases. However, our results sufficiently justify the optimisation of the H atoms from X-ray diffraction data due to the observed

changes to computed intermolecular interactions that can play a critical role in the computed thermal integrity of these charge propagation channels. In relation to the plethora of intermolecular interactions investigated herein, we anticipate our results to be of interest beyond architectures bearing the DPP core and as a result hope that this study should be of interest to material scientists interested in the rational development of superior alternatives to current organic semiconductors.

SUPPORTING INFORMATION

Full details of computed intermolecular interactions, charge transfer integrals for X-ray and H-optimised geometries as well as capped stick illustrations for all investigated dimer pairs.

AUTHOR INFORMATION

Corresponding Authors

*E-mail: j.calvo-castro@herts.ac.uk

Notes

The authors declare no competing financial interest.

REFERENCES

(1)   Černý, J.; Hobza, P. Non-Covalent Interactions in Biomacromolecules. *Physical Chemistry Chemical Physics* **2007**, *9* (39), 5291–5303. https://doi.org/10.1039/b704781a.

(2)   Ronconi, L.; Sadler, P. J. Using Coordination Chemistry to Design New Medicines. *Coordination Chemistry Reviews* **2007**, *251* (13-14 SPEC. ISS.), 1633–1648. https://doi.org/10.1016/j.ccr.2006.11.017.

(3)   Hobza, P. Calculations on Noncovalent Interactions and Databases of Benchmark Interaction Energies. *Accounts of Chemical Research* **2012**, *45* (4), 663–672. https://doi.org/10.1021/ar200255p.

(4)   Riley, K. E.; Hobza, P. Investigations into the Nature of Halogen Bonding Including Symmetry Adapted Perturbation Theory Analyses. *Journal of Chemical Theory and Computation* **2008**, *4* (2), 232–242. https://doi.org/10.1021/ct700216w.

(5)   Calvo-Castro, J.; McHugh, C. J. Exploring Structure Based Charge Transport Relationships in Phenyl Diketopyrrolopyrrole Single Crystals Using a 2D [Small Pi]-[Small Pi] Dimer Model System. *Journal of Materials Chemistry C* **2017**, *5* (16), 3993–3998. https://doi.org/10.1039/C7TC00434F.

(6)   Vura-Weis, J.; Ratner, M. A.; Wasielewski, M. R. Geometry and Electronic Coupling in Perylenediimide Stacks: Mapping Structure-Charge Transport Relationships. *Journal of the American Chemical Society* **2010**, *132* (6), 1738-+. https://doi.org/10.1021/ja907761e.

(7)   Ryno, S. M.; Risko, C.; Bredas, J.-L. Non-Covalent Interactions and Impact of Charge Penetration Effects in Linear Oligoacene Dimers and Single Crystals. *Chemistry of Materials* **2016**. https://doi.org/10.1021/acs.chemmater.6b01340.

(8)   Desiraju, G. R.; Steiner, T. *The Weak Hydrogen Bond in Structural Chemistry and Biology* **1999**.

(9)   Deringer, V. L.; Hoepfner, V.; Dronskowski, R. Accurate Hydrogen Positions in Organic Crystals: Assessing a Quantum-Chemical Aide. *Crystal Growth & Design* **2012**, *12* (2), 1014–1021. https://doi.org/10.1021/cg201505n.

(10)   Deringer, V. L.; George, J.; Dronskowski, R.; Englert, U. Plane-Wave Density Functional Theory Meets Molecular Crystals: Thermal Ellipsoids and Intermolecular Interactions. *Accounts of Chemical Research* **2017**, *50* (5), 1231–1239. https://doi.org/10.1021/acs.accounts.7b00067.

(11)   Dittrich, B.; Lübben, J.; Mebs, S.; Wagner, A.; Luger, P.; Flaig, R. Accurate Bond Lengths to Hydrogen Atoms from Single-Crystal X-Ray Diffraction by Including Estimated Hydrogen ADPs and Comparison to Neutron and QM/MM Benchmarks. *Chemistry - A European Journal* **2017**, *23* (19), 4605–4614. https://doi.org/10.1002/chem.201604705.

(12)   Steiner, T. The Hydrogen Bond in the Solid State. *Angewandte Chemie - International Edition* **2002**, *41* (1), 48–76. https://doi.org/10.1002/1521-3773(20020104)41:1<48::AID-ANIE48>3.0.CO;2-U.

(13)   Malaspina, L. A.; Edwards, A. J.; Woińska, M.; Jayatilaka, D.; Turner, M. J.; Price, J. R.; Herbst-Irmer, R.; Sugimoto, K.; Nishibori, E.; Grabowsky, S. Predicting the Position of the Hydrogen Atom in the Short Intramolecular Hydrogen Bond of the Hydrogen Maleate Anion from Geometric Correlations. *Crystal Growth and Design* **2017**, *17* (7), 3812–3825. https://doi.org/10.1021/acs.cgd.7b00390.

(14)   Sheldrick, G. M. A Short History of SHELX. *Acta Crystallographica Section A* **2008**, *64*, 112–122. https://doi.org/10.1107/s0108767307043930.

(15)   Allen, F. H.; Bruno, I. J. Bond Lengths in Organic and Metal-Organic Compounds Revisited: X - H Bond Lengths from Neutron Diffraction Data. *Acta Crystallographica Section B: Structural Science* **2010**, *66* (3), 380–386. https://doi.org/10.1107/S0108768110012048.

(16)   Hoser, A. A.; Dominiak, P. M.; Woniak, K. Towards the Best Model for H Atoms in Experimental Charge-Density Refinement. *Acta Crystallographica Section A: Foundations of Crystallography* **2009**, *65* (4), 300–311. https://doi.org/10.1107/S0108767309019862.

(17)   Jayatilaka, D.; Dittrich, B. X-Ray Structure Refinement Using Aspherical Atomic Density Functions Obtained from Quantum-Mechanical Calculations. *Acta Crystallographica Section A:*

Foundations   of   Crystallography **2008**, *64* (3), 383–393. https://doi.org/10.1107/S0108767308005709.

(18)   Capelli, S. C.; Bürgi, H.-B.; Dittrich, B.; Grabowsky, S.; Jayatilaka, D. Hirshfeld Atom Refinement. *IUCrJ* **2014**, *1*, 361–379. https://doi.org/10.1107/S2052252514014845.

(19)   Calvo-Castro, J.; Morris, G.; Kennedy, A. R.; McHugh, C. J. Effects of Fluorine Substitution on the Intermolecular Interactions, Energetics, and Packing Behavior of N-Benzyl Substituted Diketopyrrolopyrroles. *Crystal Growth & Design* **2016**, *16* (4), 2371–2384. https://doi.org/10.1021/acs.cgd.6b00157.

(20)   Calvo-Castro, J.; Morris, G.; Kennedy, A. R.; McHugh, C. J. Fluorine Directed Two-Dimensional Cruciform π–π Stacking in Diketopyrrolopyrroles. *Crystal Growth & Design* **2016**, *16* (9), 5385–5393. https://doi.org/10.1021/acs.cgd.6b00887.

(21)   Calvo-Castro, J.; Warzecha, M.; Kennedy, A. R.; McHugh, C. J.; McLean, A. J. Impact of Systematic Structural Variation on the Energetics of π–π Stacking Interactions and Associated Computed Charge Transfer Integrals of Crystalline Diketopyrrolopyrroles. *Crystal Growth & Design* **2014**, *14* (9), 4849–4858. https://doi.org/10.1021/cg5010165.

(22)   Calvo-Castro, J.; Warzecha, M.; Oswald, I. D. H.; Kennedy, A. R.; Morris, G.; McLean, A. J.; McHugh, C. J. Intermolecular Interactions and Energetics in the Crystalline π–π Stacks and Associated Model Dimer Systems of Asymmetric Halogenated Diketopyrrolopyrroles. *Crystal Growth & Design* **2016**, *16* (3), 1531–1542. https://doi.org/10.1021/acs.cgd.5b01656.

(23)   Calvo-Castro, J.; Maczka, S.; Thomson, C.; Morris, G.; Kennedy, A. R.; McHugh, C. J. Twist and Shout: A Surprising Synergy between Aryl and N-Substituents Defines the Computed

Charge Transport Properties in a Series of Crystalline Diketopyrrolopyrroles. *CrystEngComm* **2016**, *18* (48), 9382–9390. https://doi.org/10.1039/C6CE02261H.

(24)   Warzecha, M.; Calvo-Castro, J.; Kennedy, A. R.; Macpherson, A. N.; Shankland, K.; Shankland, N.; McLean, A. J.; McHugh, C. J. Detection of Nitroaromatic Vapours with Diketopyrrolopyrrole Thin Films: Exploring the Role of Structural Order and Morphology on Thin Film Properties and Fluorescence Quenching Efficiency. *Chemical Communications* **2015**, *51* (6), 1143–1146. https://doi.org/10.1039/c4cc08468c.

(25) Mizuguchi, J.; Grubenmann, A.; Rihs, G. STRUCTURES OF 3,6-BIS(3-CHLOROPHENYL)PYRROLO 3,4-C PYRROLE-1,4-DIONE AND 3,6-BIS(4-CHLOROPHENYL)PYRROLO 3,4-C PYRROLE-1,4-DIONE. *Acta Crystallographica Section B-Structural Science* **1993**, *49*, 1056–1060. https://doi.org/10.1107/s0108768193007645.

(26) Mizuguchi, J.; Grubenmann, A.; Wooden, G.; Rihs, G. STRUCTURES OF 3,6-DIPHENYLPYRROLO 3,4-C PYRROLE-1,4-DIONE AND 2,5-DIMETHYL-3,6-DIPHENYLPYRROLO 3,4-C PYRROLE-1,4-DIONE. *Acta Crystallographica Section B-Structural Science* **1992**, *48*, 696–700. https://doi.org/10.1107/s0108768192003033.

(27) Mizuguchi, J.; Miyazaki, T. Crystal Structure of 3,6-Bis(4-Biphenylyl)Pyrrolo 3,4-c Pyrrole-1,4-Dione, C30H20N2O2. *Zeitschrift Fur Kristallographie-New Crystal Structures* **2002**, *217* (1), 43–44.

(28)   Zhao, Y.; Truhlar, D. G. The M06 Suite of Density Functionals for Main Group Thermochemistry, Thermochemical Kinetics, Noncovalent Interactions, Excited States, and Transition Elements: Two New Functionals and Systematic Testing of Four M06-Class

Functionals and 12 Other Functionals. *Theoretical Chemistry Accounts* **2008**, *120* (1–3), 215–241. https://doi.org/10.1007/s00214-007-0310-x.

(29)   Shao, Y.; Molnar, L. F.; Jung, Y.; Kussmann, J.; Ochsenfeld, C.; Brown, S. T.; Gilbert, A. T. B.; Slipchenko, L. V.; Levchenko, S. V.; O'Neill, D. P.; et al. Advances in Methods and Algorithms in a Modern Quantum Chemistry Program Package. *Physical Chemistry Chemical Physics* **2006**, *8* (27), 3172–3191. https://doi.org/10.1039/b517914a.

(30)   Boys, S. F.; Bernardi, F. The Calculation of Small Molecular Interactions by the Differences of Separate Total Energies. Some Procedures with Reduced Errors (Reprinted from Molecular Physics, Vol 19, Pg 553-566, 1970). *Molecular Physics* **2002**, *100* (1), 65–73. https://doi.org/10.1080/00268970110088901.

(31)   Bredas, J. L.; Beljonne, D.; Coropceanu, V.; Cornil, J. Charge-Transfer and Energy-Transfer Processes in Pi-Conjugated Oligomers and Polymers: A Molecular Picture. *Chemical Reviews* **2004**, *104* (11), 4971–5003. https://doi.org/10.1021/cr040084k.

(32)   Hao, Z. M.; Iqbal, A. Some Aspects of Organic Pigments. *Chemical Society Reviews* **1997**, *26* (3), 203–213. https://doi.org/10.1039/cs9972600203.

(33)   Herbst, W.; Hunger, K. *Industrial Organic Pigments*; Wiley-VCH, 2004.

(34)   Wallquist, O.; Lenz, R. 20 Years of DPP Pigments - Future Perspectives. *Macromolecular Symposia* **2002**, *187*, 617–629. https://doi.org/10.1002/1521-3900(200209)187:1<617::aid-masy617>3.0.co;2-5.

(35)   Uttiya, S.; Miozzo, L.; Fumagalli, E. M.; Bergantin, S.; Ruffo, R.; Parravicini, M.; Papagni, A.; Moret, M.; Sassella, A. Connecting Molecule Oxidation to Single Crystal Structural and

Charge Transport Properties in Rubrene Derivatives. *J. Mater. Chem. C* **2014**, *2* (21), 4147–4155. https://doi.org/10.1039/C3TC32527J.

(36) Braga Daniele; Jaafari Abdelhafid; Miozzo Luciano; Moret Massimo; Rizzato Silvia; Papagni Antonio; Yassar Abderrahim. The Rubrenic Synthesis: The Delicate Equilibrium between Tetracene and Cyclobutene. *European Journal of Organic Chemistry* **2011**, *2011* (22), 4160–4169. https://doi.org/10.1002/ejoc.201100033.

(37) Xie, W.; Prabhumirashi, P. L.; Nakayama, Y.; McGarry, K. A.; Geier, M. L.; Uragami, Y.; Mase, K.; Douglas, C. J.; Ishii, H.; Hersam, M. C.; et al. Utilizing Carbon Nanotube Electrodes to Improve Charge Injection and Transport in Bis(Trifluoromethyl)-Dimethyl-Rubrene Ambipolar Single Crystal Transistors. *ACS Nano* **2013**, *7* (11), 10245–10256. https://doi.org/10.1021/nn4045694.

(38) Ogden, W. A.; Ghosh, S.; Bruzek, M. J.; McGarry, K. A.; Balhorn, L.; Young, V.; Purvis, L. J.; Wegwerth, S. E.; Zhang, Z.; Serratore, N. A.; et al. Partial Fluorination as a Strategy for Crystal Engineering of Rubrene Derivatives. *Crystal Growth & Design* **2017**, *17* (2), 643–658. https://doi.org/10.1021/acs.cgd.6b01497.

(39) Paraskar Abhimanyu S.; Reddy A. Ravikumar; Patra Asit; Wijsboom Yair H.; Gidron Ori; Shimon Linda J. W.; Leitus Gregory; Bendikov Michael. Rubrenes: Planar and Twisted. *Chemistry – A European Journal* **2008**, *14* (34), 10639–10647. https://doi.org/10.1002/chem.200800802.

(40) Sakamoto, Y.; Suzuki, T. Perfluorinated and Half-Fluorinated Rubrenes: Synthesis and Crystal Packing Arrangements. *J. Org. Chem.* **2017**, *82* (15), 8111–8116. https://doi.org/10.1021/acs.joc.7b01383.

(41)   McGarry, K. A.; Xie, W.; Sutton, C.; Risko, C.; Wu, Y.; Young, V. G., Jr.; Bredas, J.-L.; Frisbie, C. D.; Douglas, C. J. Rubrene-Based Single-Crystal Organic Semiconductors: Synthesis, Electronic Structure, and Charge-Transport Properties. *Chemistry of Materials* **2013**, *25* (11), 2254–2263. https://doi.org/10.1021/cm400736s.

(42)   Reichenbacher, K.; Suss, H. I.; Hulliger, J. Fluorine in Crystal Engineering - "the Little Atom That Could." *Chemical Society Reviews* **2005**, *34* (1), 22–30. https://doi.org/10.1039/b406892k.

(43)   Dunitz, J. D.; Taylor, R. Organic Fluorine Hardly Ever Accepts Hydrogen Bonds. *Chemistry-a European Journal* **1997**, *3* (1), 89–98. https://doi.org/10.1002/chem.19970030115.

(44)   Dunitz, J. D. Organic Fluorine: Odd Man Out. *Chembiochem* **2004**, *5* (5), 614–621. https://doi.org/10.1002/cbic.200300801.

(45)   Nayak, S. K.; Reddy, M. K.; Row, T. N. G.; Chopra, D. Role of Hetero-Halogen (F Center Dot Center Dot Center Dot X, X = Cl, Br, and I) or Homo-Halogen (X Center Dot Center Dot Center Dot X, X = F, Cl, Br, and I) Interactions in Substituted Benzanilides. *Crystal Growth & Design* **2011**, *11* (5), 1578–1596. https://doi.org/10.1021/cg101544z.

(46)   Chopra, D.; Row, T. N. G. Role of Organic Fluorine in Crystal Engineering. *Crystengcomm* **2011**, *13* (7), 2175–2186. https://doi.org/10.1039/c0ce00538j.

(47)   Berger, R.; Resnati, G.; Metrangolo, P.; Weber, E.; Hulliger, J. Organic Fluorine Compounds: A Great Opportunity for Enhanced Materials Properties. *Chemical Society Reviews* **2011**, *40* (7), 3496–3508. https://doi.org/10.1039/c0cs00221f.

(48) Fu, C.; Belanger-Gariepy, F.; Perepichka, D. F. Supramolecular Ordering of Difuryldiketopyrrolopyrrole: The Effect of Alkyl Chains and Inter-Ring Twisting. *CrystEngComm* **2016**, *18* (23), 4285–4289. https://doi.org/10.1039/C6CE00383D.

(49) Sevincek, R.; Celik, S.; Aygun, M.; Alp, S.; Isik, S. 2,5-Dihexyl-3,6-Diphenylpyrrolo[3,4-c]Pyrrole-1,4(2H,5H)-Dione. *Acta Crystallographica Section E* **2010**, *66* (7), o1546. https://doi.org/10.1107/S1600536810020398.

(50) Naik, M. A.; Venkatramaiah, N.; Kanimozhi, C.; Patil, S. Influence of Side-Chain on Structural Order and Photophysical Properties in Thiophene Based Diketopyrrolopyrroles: A Systematic Study. *Journal of Physical Chemistry C* **2012**, *116* (50), 26128–26137. https://doi.org/10.1021/jp306365q.

(51) Li, Y.; Sonar, P.; Murphy, L.; Hong, W. High Mobility Diketopyrrolopyrrole (DPP)-Based Organic Semiconductor Materials for Organic Thin Film Transistors and Photovoltaics. *Energy & Environmental Science* **2013**, *6* (6), 1684–1710. https://doi.org/10.1039/c3ee00015j.

TOC Graphic